Magnetic Resonance Imaging of Unusual Neoplasms Related to Foramen of Luschka: A Review for Differential Diagnosis

Mustafa Kemal Demir[1] Umut Özdamarlar[1] Baran Yılmaz[2] Akın Akakın[2] Turker Kılıc[2]

[1] Department of Radiology, Bahçeşehir University School of Medicine, Göztepe Medical Park Training and Education Hospital, Istanbul, Turkey
[2] Department of Neurosurgery, Bahçeşehir University School of Medicine, Göztepe Medical Park Training and Education Hospital, Istanbul, Turkey

Address for correspondence Mustafa Kemal Demir, MD, 11. Kisim, Yasemin Apt, D Blok, Daire 35 Ataköy, Istanbul, Turkey 34158 (e-mail: demir.m.k@gmail.com).

Indian J Radiol Imaging 2022;32:71–80.

Abstract

There are many types of neoplasms in or around the foramen of Luschka (FL), and definitive diagnosis in some cases requires knowledge of imaging findings. The uncommon and challenging neoplasms with FL involvement considered in this study are exophytic brainstem glioma, primary glioblastoma of the cerebellopontine angle (CPA), primary anaplastic ependymoma of the CPA, choroid plexus papilloma of the FL, solitary FL choroid plexus metastasis, extraskeletal myxoid chondrosarcoma of the jugular foramen, paraganglioma of the jugular foramen, exostosis of the jugular foramen, psammomatous meningioma in the lateral cerebellar medullary cistern, epidermoid tumor of the fourth ventricle, and a hypoglossal schwannoma. These neoplasms may have overlapping clinical and imaging features, but some have relatively distinct imaging features. Knowledge of the key clinical and magnetic resonance imaging features of these unusual lesions with FL involvement is important for radiologists to improve diagnostic ability and to assist the referring physician in the appropriate management of the patient.

Keywords
- neoplasms
- posterior fossa
- foramen of Luschka
- magnetic resonance imaging

Introduction

Magnetic resonance imaging (MRI) is the most important imaging modality for the diagnosis and follow-up of lesions in or around the foramen of Luschka (FL). These lesions may present with different clinical appearances depending on their size and origin. However, diagnosis can be complicated by the atypical appearance, rarity, and overlapping symptomatology. To determine the appropriate treatment for the patient, it is critical to determine the anatomic extent and key imaging features of the neoplasm.

In this study, we present a series of unusual neoplasms related to FL with a review of the clinicoradiologic differential diagnosis that will help radiologists improve their ability to make a correct diagnosis noninvasively. A brief description of the embryology and anatomy of FL is also included. It should be noted that there are many other more common

published online
April 19, 2022

DOI https://doi.org/10.1055/s-0042-1743113.
ISSN 0971-3026.

Thieme Medical and Scientific Publishers Pvt. Ltd., A-12, 2nd Floor, Sector 2, Noida-201301 UP, India

tumoral or nontumoral space-occupying lesions that are not mentioned in this text.

Embryology

The neural tube develops at about the fourth week of gestation. The fourth ventricle develops in the first trimester of pregnancy as a large primordium from the cavity or part of the neural tube of the hindbrain. The cerebellum develops over a long period of time, during which the fourth ventricle shrinks. Lateral recesses begin to form around the seventh week. There is no consensus on the development of FL. A period between 26 weeks and a few hours before birth has been cited.[1]

Anatomy

The FL is the lateral aperture of the fourth ventricle. It is a natural opening between the lateral recess of the fourth ventricle and the subarachnoid space at the lateral cerebellomedullary cistern through which cerebrospinal fluid (CSF) circulates. It has anterior, lateral, posterior, and inferior portions. It opens superolaterally into the cerebellopontine cistern. The facial nerve and vestibulocochlear nerve arise at the lateral end immediately rostral to the FL. At the level of the medial part of the FL, the pons and medulla are separated by the sulcus pontomedullaris. The trigeminal nerve arises in the midpons and the abducens nerve in the medial part of the pontomedullary sulcus. The inferior part is adjacent to the inferior cerebellar peduncle, the accessory nucleus of the cuneate, and the superior part of the hypoglossal nucleus. Inferior and slightly anterior to the FL is the *olive*. The hypoglossal nucleus is located in the medulla near the midline. The hypoglossal nerve exits the medulla oblongata between the olive and the pyramid from the preolivary sulcus and passes through the hypoglossal canal. The glossopharyngeal, vagus, and accessory nerves emerge from the retro-olivary groove, forming a continuous line of nerve roots. The choroid plexus of the fourth ventricle projects into the FL and cerebellopontine cisterna behind the glossopharyngeal and vagus nerves. The anterior part lies close to the vestibulocochlear nerve and facial nerve with the choroid plexus (►**Fig. 1**). The FLs can be easily assessed with MRI (►**Fig. 2**).

Clinical Presentation

Most lesions associated with FL are lesions of the cerebellopontine angle (CPA). Therefore, patients usually present with ataxia and paralysis of the fifth, seventh, or eighth cranial nerves. Hydrocephalus can result from either overproduction of CSF or an obstruction of the outflow of the fourth ventricle and presents with the typical clinical features of headache, nausea, and vomiting. Acute hydrocephalus can lead to impaired consciousness. FL may also be affected by the neoplastic lesions of the inferior cranial nerves, and patients may present with symptoms related to important functions such as swallowing, tasting, speaking, heart rate and blood pressure control, and peristalsis.

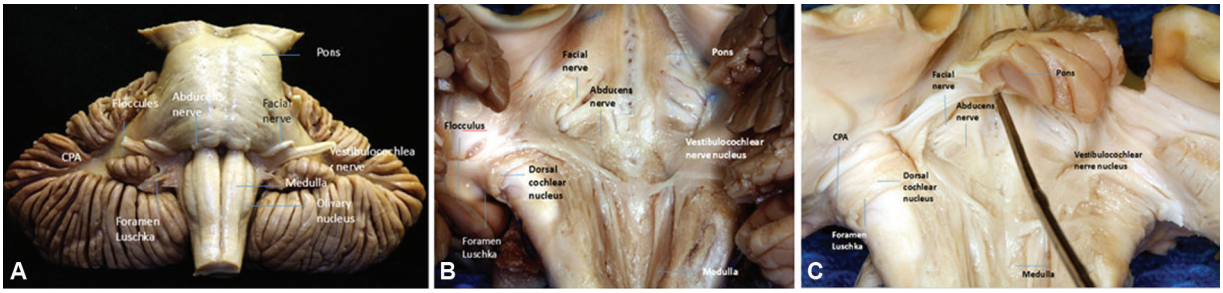

Fig. 1 Cadaveric images with labels from ventral (**A**), dorsal (**B**), and lateral (**C**) views of brainstem and cerebellum, showing the foramen of Luschka and adjacent anatomic structures.

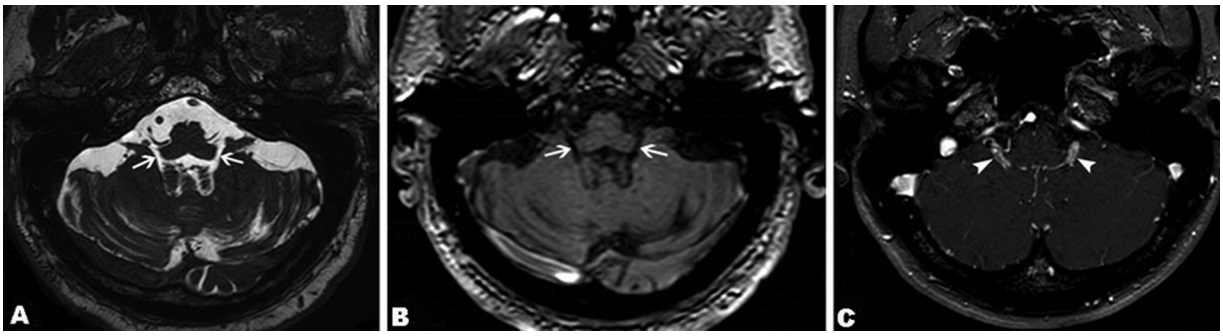

Fig. 2 Normal appearance of foramens of Luschka (FLs) on axial three-dimensional (3D) balanced fast field echo (FFE) image (**A**) and 3D FFE T1-weighted (**B**) magnetic resonance (MR) images (arrows). Gadolinium-enhanced axial 3D FFE T1-weighted MR image (**C**) reveals enhancing choroid plexus of the FLs (arrows).

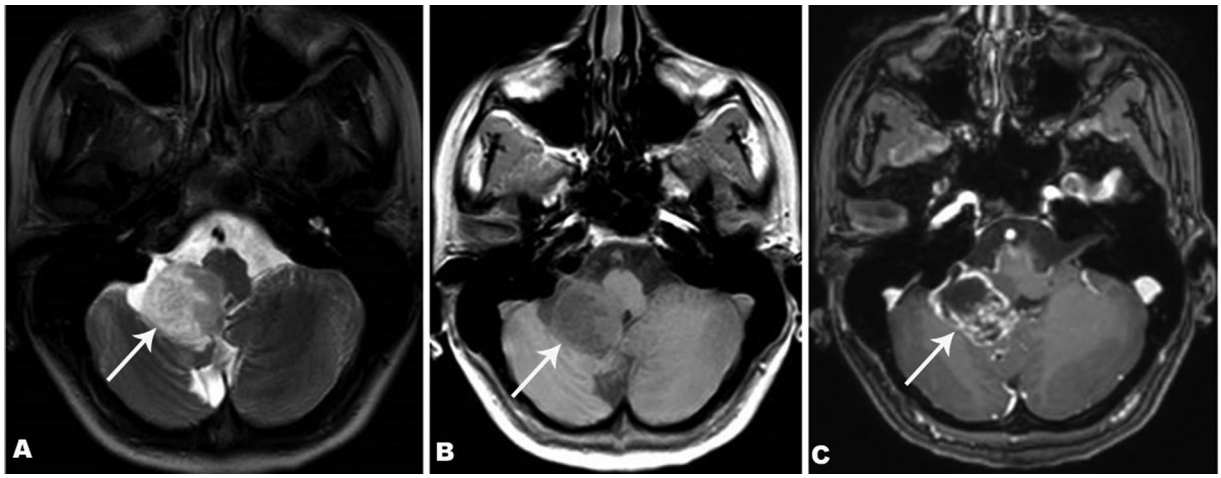

Fig. 3 Magnetic resonance imaging of a focal brainstem glioma (pilocytic astrocytoma) in a 17-year-old female with headache, vertigo, and ataxia. (**A**) Transverse T2-weighted image reveals a heterogeneously hyperintense posterior fossa mass centered within the left cerebellomedullary area, invading the foramen of Luschka with extension from the left lateral recess of the fourth ventricle into the left cerebellopontine angle (arrow). (**B**) The tumor shows heterogeneously hypointense signals on transverse unenhanced T1-weighted image (arrow). (**C**) Tumor shows heterogeneous enhancement on transverse gadolinium-enhanced T1-weighted image (arrow).

Magnetic Resonance Imaging

MRI is the primary imaging modality of choice in the evaluation of neoplasms involving FL. It provides the best soft tissue contrast, is multiplanar, and does not use ionizing radiation. MRI can easily assess tumors of vascular origin, vascular structures, and the vascularity of neoplasms. It is primarily used to characterize neoplasms, including assessment of signal intensity, size, morphology, location, and relationship to adjacent structures such as arteries, veins, nerves, and FL. Detection of fat, blood products, fluid, and relationships to bony structures provides important key findings for noninvasive diagnosis.

The essential components of the basic MRI protocol include T1-weighted (w), T2-w, and fluid attenuation inversion recovery (FLAIR) sequences; contrast-enhanced T1-w imaging; susceptibility-weighted imaging; diffusion-weighted imaging (DWI); and magnetic resonance (MR) angiography. MR spectroscopy (MRS), diffusion tensor tractography, and perfusion MRI are the advanced imaging modalities useful in imaging differential diagnosis. Observation of marked restricted diffusion in a mass in the posterior fossa mass on DWI helps in the diagnosis of medulloblastoma and epidermoid tumor. MRS plays an important role in the differential diagnosis between non-neoplastic and neoplastic lesions, as well as benign and malignant brain lesions.[2] Moreover, a taurine peak at 3.35 ppm, a myo-inositol peak at 3.5 ppm, and a decrease in creatinine (Cr) at 3.03 ppm are highly suggestive of medulloblastoma, ependymoma, and pilocytic astrocytoma (PA), respectively.[3]

Exophytic Focal Brainstem Glioma

These tumors may arise from the subependymal glial tissue on the dorsal surface of the inferior brainstem and spread "exophytically" into the perimedullary cisterns rather than infiltrate the adjacent brainstem. When located eccentrically near the lateral recess of the fourth ventricle, they may fill the FL. The majority are low-grade tumors, with most tumors being PAs. Gangliogliomas, oligodendrogliomas, fibrillary astrocytomas, and glioblastomas may also occur.[4,5] The tegmentum, brachium pontis, and lateral part of the medulla are the preferred sites. Because the III–XII cranial nerves contain oligodendrocytes that extend to the cranial nerve segments, these brainstem gliomas may affect cranial nerves and be misdiagnosed as extra-axial tumors with perineural spread. These tumors are usually homogeneous and well demarcated with cystic remodeling. The presence of necrotic or hemorrhagic components and diffusion restriction is uncommon. The enhancement pattern is variable and may mimic an aggressive tumor (►**Fig. 3**). Follow-up time is a very important consideration point as it indicates a slower growth rate. Imaging differential diagnoses include medulloblastoma, brain metastases, ependymoma, and primary parenchymal lymphoma.[6] Ipsilateral cerebellar atrophy has been found in brainstem gangliogliomas.[7]

Proton MRS and perfusion imaging are useful to detect low-grade focal exophytic brainstem tumors that have lower choline (Cho) peak, low Cho/Cr and Cho/*N*-acetylaspartate (NAA) ratios, and lower blood volume. Diagnosis of focal PA in the brainstem can be problematic because of its variable conventional and perfusion MRI features. These tumors may have indistinct margins and may bleed. DWI helps in the differential diagnosis when there is peripheral enhancement mimicking an abscess. The solid component of PAs usually does not show restricted diffusion and has higher apparent diffusion coefficient values than other cerebellar tumors. On MRS, Cho is typically very high in pilocytic tumors along with lipids and lactate peaks. In addition, PAs can sometimes show high blood volume on perfusion imaging.[8,9]

Primary Glioblastoma of Cerebellopontine Angle

A primary glioblastoma in the CPA is extremely rare, with only ten cases published so far.[10] The origin of the tumor may be

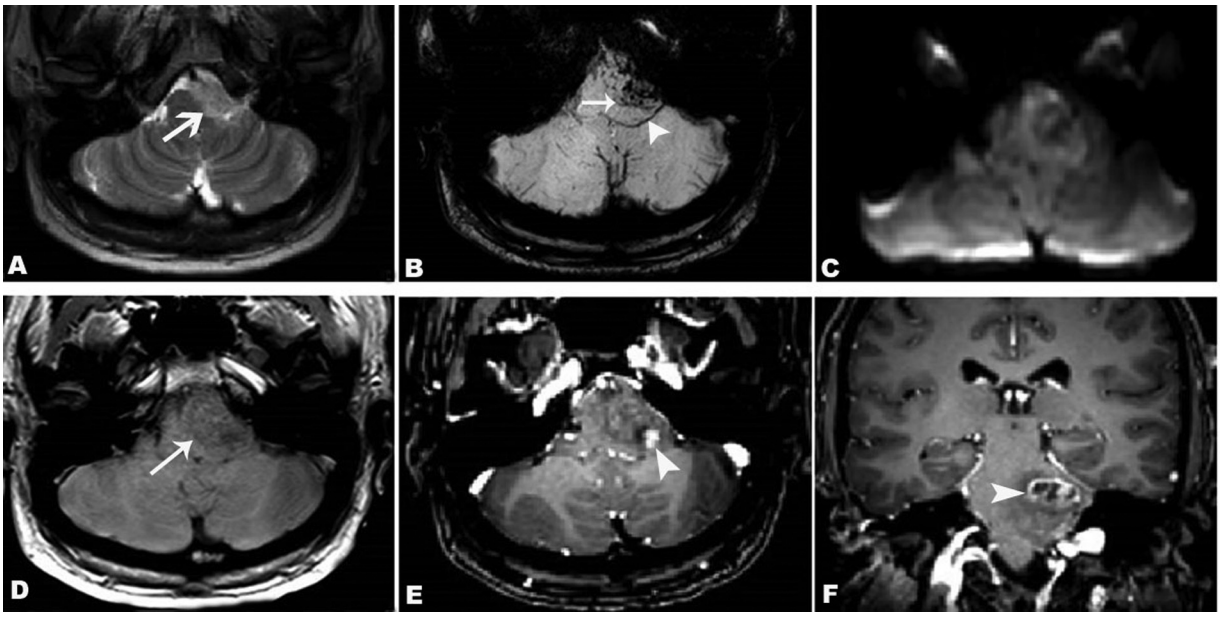

Fig. 4 Magnetic resonance imaging of a pathologically confirmed primary cerebellopontine angle (CPA) glioblastoma in a 27-year-old male patient with progressive headache, nausea, vomiting, and ataxia. (**A**) On the axial T2-weighted image, the left CPA tumor reveals low and high signals. Invasion of left foramen of Luschka (FL) is clearly observed (arrow). (**B**) Axial susceptibility-weighted minIP image shows markedly hypointense signal consistent with intratumoral hemorrhage (arrow). Thickened and marked hypointense left FL with posterior displacement is seen due to invasion and fluid/hemorrhage (arrowhead). (**C**) Diffusion-weighted imaging reveals heterogeneous diffusion abnormality. (**D**) The tumor shows heterogeneous low signals on unenhanced T1-weighted image (arrow). (**E**) Axial and (**F**) coronal postcontrast T1-weighted images show irregular heterogeneous enhancement (arrowheads).

cranial nerve VIII or V, or it may arise from heterotopic neuroglial cell nests in the leptomeninges. Owing to its aggressive course, the involvement of FL may exist easily. MRI findings are similar to those in neural parenchyma and typically include heterogeneous low signals on T1 and high signals on T2-w images. There may be cystic–necrotic and hemorrhagic areas in the tumor. The enhancement is usually irregular and ringlike. Perifocal edema has been almost always present (►**Fig. 4**).[10] The main differential diagnosis may include metastases, abscess, hemangioblastoma, cystic astrocytoma, encephalitis, granulomas, or tumefactive multiple sclerosis. In glioblastoma, the Cho/Cr ratio is found to increase over 3:1, and the NAA peak is reduced. Cho concentration is reduced in low-grade gliomas and infections. The presence of vascularity and increased relative cerebral blood volumes on perfusion-weighted MRI and metabolite levels on MRS in the periphery of the tumor are helpful in the differential diagnosis of metastases and glioblastoma. Tumefactive multiple sclerosis and granulomas are usually encountered with other lesions either located in the cerebellar and cerebral hemispheres or brainstem.[11,12] Neither the clinical features nor the imaging findings may be enough to make a correct preoperative diagnosis.

Primary Anaplastic Ependymoma of the Cerebellopontine Angle

Atypical posterior fossa ependymoma typically arises in the fourth ventricle. The tumor's extension into the CPA and the subarachnoid spaces through the FLs or Magendie is well documented in the literature. However, a primary extra-axial CPA location may rarely occur due to the persistence of glial rests in the cerebellomedullary cistern, cerebellopontine cistern, or in the FL.[13] This location is very rare in adults and creates a diagnosing challenge.[14] Ependymomas are generally seen as lobulated solid tumors, which are hypointense on T1-w image, hyperintense on T2-w image, and demonstrate intense irregular enhancement on MRI. They may show heterogeneity due to necrosis, cystic components, calcification, or hemorrhage. It is not typically accompanied by hearing loss (►**Fig. 5**). In the first instance, the main imaging differential diagnosis should be medulloblastoma. Ependymomas are prone to extending through the FL and Magendie. However, medulloblastomas do not tend to extend through foramina. Medulloblastomas usually demonstrate prominent "restricted diffusion" on MRI. Calcifications and old hemorrhages, which have been reported in ~50% of ependymoma cases, result in focal hypointensities on all MRI sequences. On postcontrast MRI, ependymomas typically demonstrate heterogeneous enhancement along with faint or no enhancement, which represents areas of necrosis and intratumoral cysts. Contrast enhancement is more homogeneous in medulloblastomas. Anaplastic ependymomas may show elevated Cho and reduced NAA on MRS. Since they tend to displace the white matter tracts, diffusion tensor imaging may provide the location of tumor margins and the degree of deflection of white matter tracts. There may be elevated cerebral blood volume within the tumor on perfusion imaging.[5]

Foramen of Luschka Choroid Plexus Papilloma

Choroid plexus papillomas originate from the neuroepithelial cells of the choroid plexus. It may rarely arise

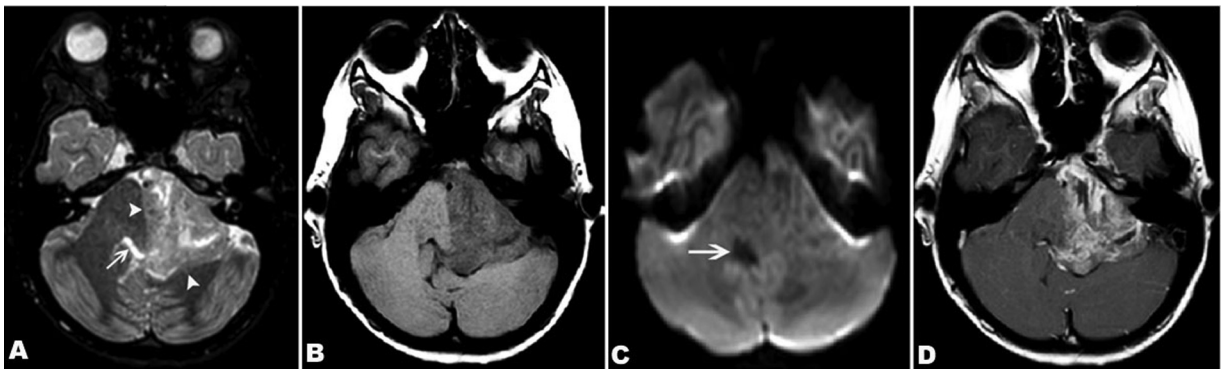

Fig. 5 Magnetic resonance imaging of a pathologically confirmed primary cerebellopontine anaplastic ependymoma (filling the left foramen of Luschka) in a 12-year-old female patient with progressive headache, vomiting, and ataxia (**A**) The tumor shows heterogeneous hyperintense signals on axial T2-weighted image, when compared with the cerebellum (arrowheads). (**B**) The tumor is heterogeneous hypointense on T1-weighted image. (**C**) There is no prominent hyperintensity on diffusion-weighted imaging, due to lack of restricted diffusion. The fourth ventricle is compressed, distorted, and shifted to the left (arrows in A–C). (**D**) The tumor shows irregular intense enhancement on gadolinium-enhanced T1-weighted image.

within the FL.[15] Although the imaging appearance is not constant, most of the cases are hypointense relative to the gray matter on T1-w images, heterogeneously hyperintense on T2-w images, and reveal intense enhancement on gadolinium-enhanced T1-w images. MRS usually demonstrates a prominent Cho peak without an NAA or Cr peak (►**Fig. 6**). The main differential diagnosis of the FL choroid plexus papilloma may include ependymoma, medulloblastoma, and meningioma. Intracranial infratentorial meningiomas without dural attachment may arise from the choroid of the fourth ventricle, inferior tela, cisterna magna, and FL.[16] The differential diagnosis between FL choroid plexus papilloma and meningioma can be particularly difficult. Characteristic imaging findings of meningiomas such as high density in the adjacent brain on computed tomography (CT), well-demarcated smooth borders, and almost homogeneous intense contrast enhancement may help in differential diagnosis. Advanced MRI techniques such as perfusion-weighted imaging could provide additional information on tumor vascularization that may help to differentiate choroid plexus carcinomas and papillomas.[17]

Solitary Choroid Plexus Metastasis of Foramen of Luschka

Apart from metastasis by neighborhood or diffuse leptomeningeal metastasis, solitary choroid plexus metastasis to the FL may occasionally occur. The most likely sources of choroid plexus metastasis are renal carcinoma and lung carcinoma. The choroid plexus of the lateral ventricles is the most common site of metastatic spread. Only 0.4% of all ventricular metastases are located in the fourth ventricle.[18] Imaging findings of a solitary metastasis to the choroid plexus may be indistinguishable from those of a neoplastic tumor such as meningioma or choroid plexus neoplasm and non-neoplastic processes such as infections (fungal, opportunistic, etc.), granulomatous processes (sarcoidosis, tuberculosis), and autoimmune or inflammatory disease. A malignant history together with postcontrast enhancement, intraventricular hemorrhage, and peritumoral edema on imaging may indicate the diagnosis (►**Fig. 7**). In these patients, the entire neuroaxis MRI examination is essential. The critical MR sequences for detecting metastasis are gadolinium-enhanced three-dimensional T1-w sequence (with multiplanar reformatted images), T2, and FLAIR.

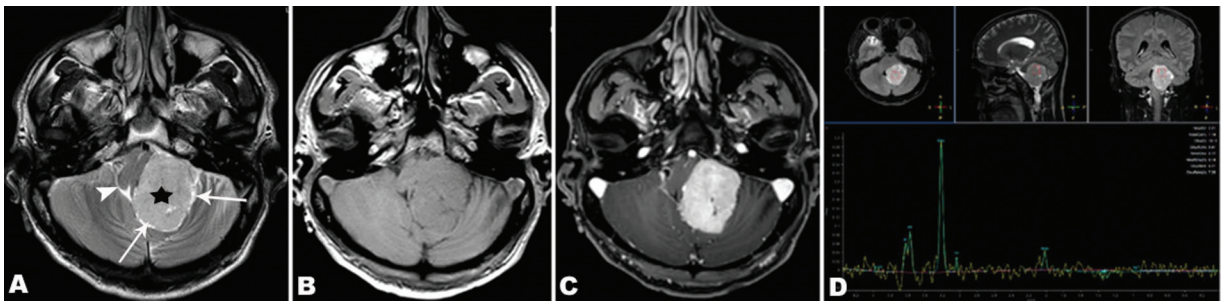

Fig. 6 Magnetic resonance imaging (MRI) of a pathologically confirmed choroid plexus papilloma in the left foramen of Luschka (FL) in a 35-year-old male patient with a 6-month history of headache and dizziness. (**A**) Transverse T2-weighted image reveals an extra-axial heterogeneous hyperintense tumor (black star), surrounded by cerebrospinal fluid (arrows). The right FL is normal (arrowhead). (**B**) Transverse T1-weighted image reveals a well-marginated tumoral mass isointense to cortical gray matter in the FL. The mass extends to the left cerebellomedullary cistern laterally and left lateral recess of the fourth ventricle medially. (**C**) The mass shows almost homogeneous intense enhancement on gadolinium-enhanced T1-weighted images (black star). The MRI findings are identical to a meningioma. (**D**) Magnetic resonance spectroscopy reveals an elevated choline peak without an *N*-acetylaspartate, creatinine peak, and alanine.

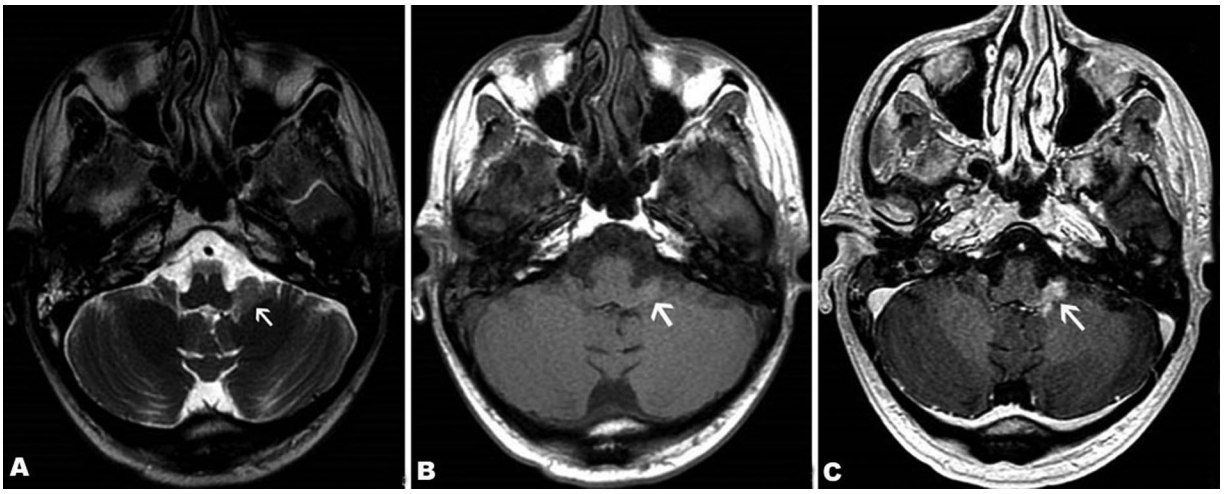

Fig. 7 Follow-up magnetic resonance imaging in a 26-year-old man with headache 13 months after surgical resection of supratentorial astroblastoma, showing a left foramen of Luschka (FL) metastasis. (**A**) Transverse T2-weighted image reveals a solid hyperintense lesion in the left FL (arrow). (**B**) The mass is isointense to the cerebellum on axial T1-weighted image (arrow). (**C**) The lesion shows intense irregular enhancement on gadolinium-enhanced transverse T1-weighted image (arrow).

Extraskeletal Myxoid Chondrosarcoma of the Jugular Foramen

Extraskeletal myxoid chondrosarcoma is a rare mesenchymal tumor that typically originates in the deep soft tissue of the proximal extremities and limb girdles. The occurrence in the CPA or jugular foramen is sporadically encountered and may result in FL invasion.[19] MRI features are variable. These tumors appear as well-demarcated masses with smooth multilobulated margins, except in areas of osseous invasion. As they typically contain myxoid material, they show homogeneous hyperintense signals on T2-w images. They are usually isointense on T1-w images. Unlike other types of chondrosarcomas, calcification is uncommon and presents a diagnostic challenge (►**Fig. 8**). Although these tumors are generally homogeneous, they may sometimes be heterogeneous due to hemorrhagic and necrotic degeneration and calcifications. Thus, the signal characteristics may range from hypointense, isointense, or hyperintense relative to muscles or cortex on MRI. The enhancement pattern is also not constant and may show mild, moderate, or intense enhancement in contrast-enhanced imaging studies.[20] The radiologic differential diagnosis of this tumor may include a lot of other tumors such as glomus tumor, chordoma, chondroma, meningioma, myoepithelial carcinoma, and metastasis with various overlapping imaging features. Chondrosarcomas show significantly higher apparent diffusion than chordomas on DWI.[21] Angiography studies serve as a diagnostic tool with classical tumor blush in glomus tumors. Meningiomas have partial calcification and infiltration of the diploic spaces within the skull base, creating a characteristic hyperostosis. This finding is usually helpful in the differential diagnosis of meningiomas and malignant

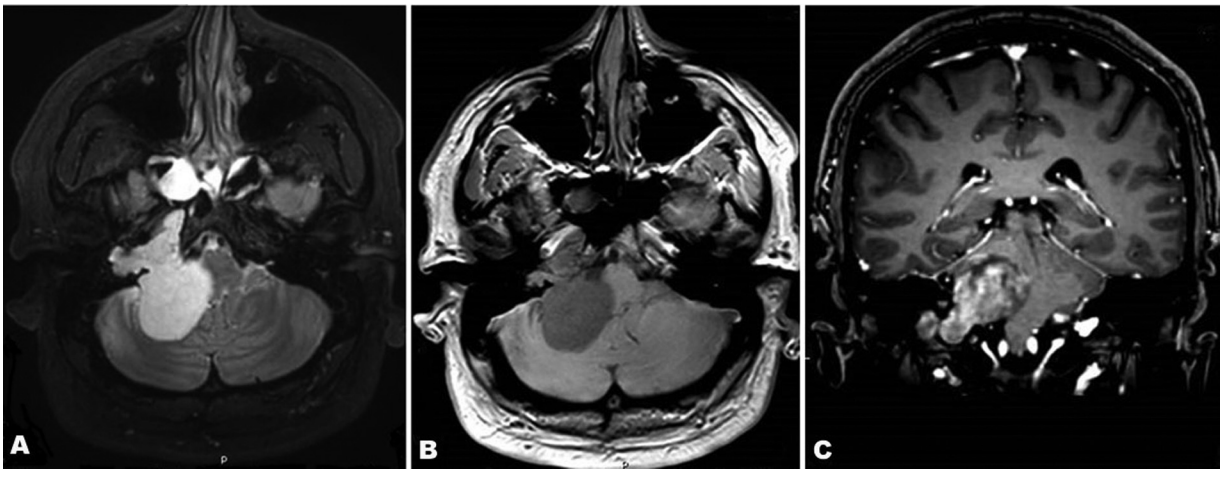

Fig. 8 Magnetic resonance imaging of a pathologically confirmed extraskeletal myxoid chondrosarcoma in a 39-year-old male patient with headache, right-sided hearing loss, and loss of balance for several months. (**A**) Transverse T2-weighted image demonstrates brightly hyperintense, multilobulated right jugular foramen mass with extension to the foramen of Luschka and cerebellopontine angle. (**B**) The tumor shows low signal on transverse T1-weighted image. (**C**) There is an inhomogeneous intense enhancement on coronal gadolinium-enhanced T1-weighted images.

lesions with bone destruction such as chondrosarcomas. Schwannomas are usually together with expansion and remodeling of the affected jugular foramen and have a characteristic dumbbell configuration.

Glomus Jugulare Paraganglioma

Glomus jugulare tumors, also known as paragangliomas and chemodectomas, originate from chemoreceptor cells in the adventitia of the jugular bulb. These hypervascular tumors are more common in females between 40 and 60 years of age. Patients with the disease most commonly present with a jugular foramen syndrome (Vernet syndrome), which is characterized by cranial nerve palsies of the glossopharyngeal, vagal, and accessory nerves. Other symptoms such as tinnitus, dizziness, hearing loss, and localized pain may also be present. They have irregular borders and are usually larger than 2 cm in size. The margins of the jugular foramen typically show irregular permeative erosion. The salt and pepper appearance with variable signals creates an MR imaging chameleon. High-velocity signal loss from flow voids causes the dark pepper and the salt to be secondary to the high signal from subacute hemorrhage on T1-w images. The tumor is isointense or mildly hyperintense on T2-w images and shows intense heterogeneous avid enhancement on postcontrast images (►**Fig. 9**).[22,23] The CT examination better demonstrates the extent of bone destruction as a "moth-eaten" pattern of erosion. Angiography shows a hypervascular mass with intense tumor blush with enlarged feeding arteries and early draining veins. Ascending pharyngeal artery is the primary arterial supply. The main differential diagnoses include meningioma, schwannoma, and metastasis. Indium-111 pentetreotide scintigraphy (octreoscan) is useful for differentiation from nerve sheath tumors, detection of multicentric or metastatic paragangliomas, and distinguishing scar from recurrence on postsurgical imaging.[24]

Jugular Tubercle Exostosis

The jugular foramen exhibits complex anatomy with its bony coverings and connections. The imaging diagnosis may be complicated when lesions originate from the petrous bone or the clivus. Chordomas, chondrosarcomas, chondroblastomas, osteoclastomas, fibrosarcomas, endolymphatic sac tumors, malignant temporal bone tumors, cholesteatoma, epidermoid tumors, cholesterol granuloma, petrositis, osteomyelitis, abscess, and mucoceles are all examples of jugular tubercle lesions.[25] However, many other extremely rare entities have also been described as having a large jugular tubercle exostosis. The jugular tubercles are two small bony protuberances that originate at the inferolateral margins of the clivus. They may vary in size and shape and may cause symptoms.[26] The imaging diagnosis can be made easily by recognizing its benign osseous growth extending outward from the surface without a cartilage cap (►**Fig. 10**). It is a

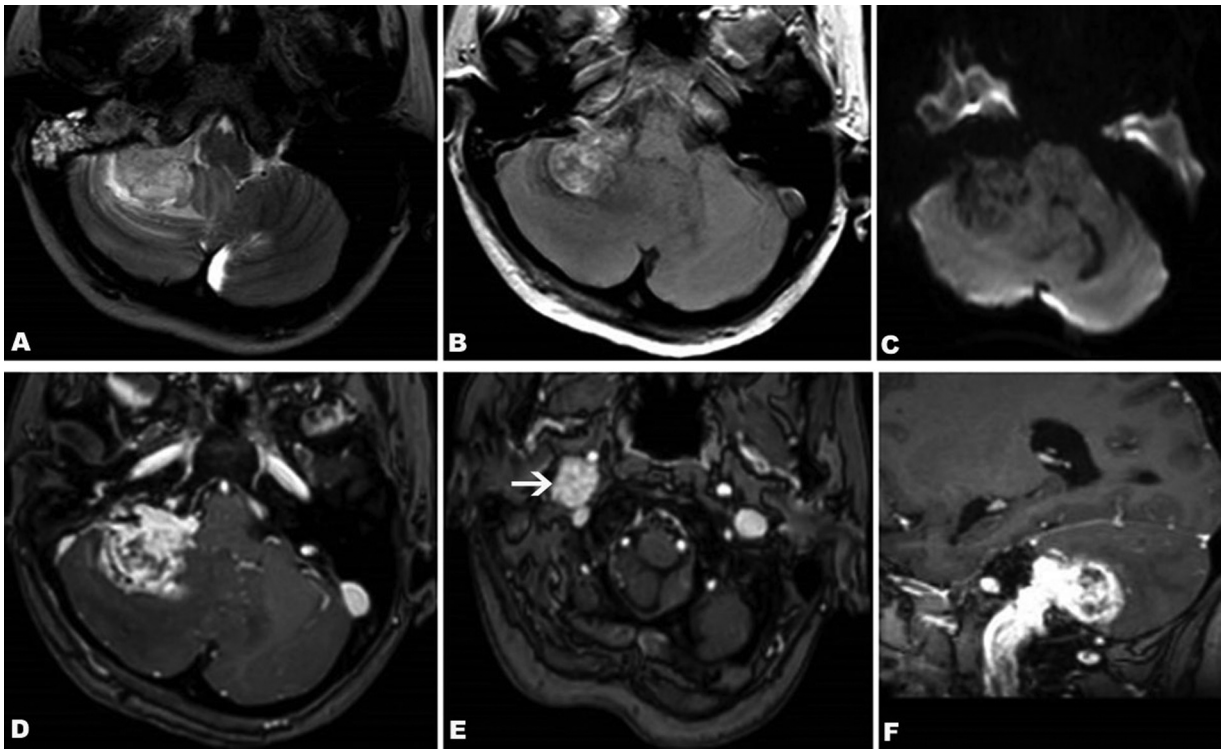

Fig. 9 Magnetic resonance imaging of a glomus jugulare paraganglioma in a 55-year-old female patient with hoarseness and vertigo. (**A**) Transverse T2-weighted image demonstrates a heterogeneous right jugular foramen mass with intracranial extension, involving foramen of Luschka. (**B**) The tumor shows heterogeneous hypointense signals due to subacute hemorrhage on transverse T1-weighted image. (**C**) There is no diffusion abnormality on diffusion-weighted imaging. (**D–F**) The tumor shows intense heterogeneous enhancement on postcontrast axial, coronal, and sagittal T1-weighted images. Internal jugular vein is compressed by the extracranial component of the tumor (arrow).

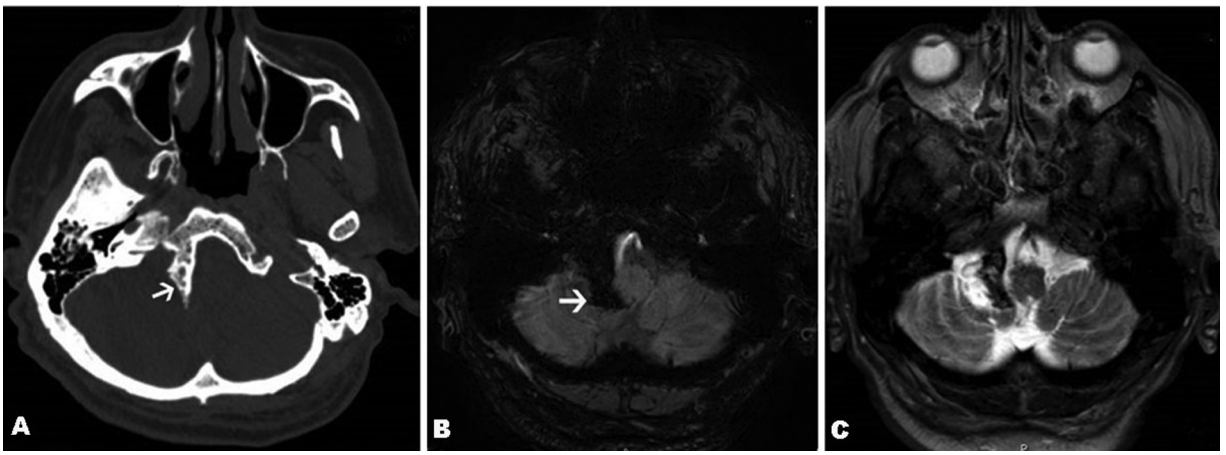

Fig. 10 Jugular tubercle exostosis in a 74-year-old male with chronic headache. Transverse "bone-window setting" computed tomography (**A**), susceptibility-weighted (**B**), and T2-weighted (**C**) magnetic resonance images through the level of foramens of Luschka (FLs) show a jugular tubercle exostosis that extends to the right FL, compressing the adjacent neural parenchymal tissues (arrows).

developmental lesion rather than a true neoplasm. They are correctly assessed with CT or MRI to detect the characteristic marrow and cortical continuity. Where exostoses are capped with cartilage, they are termed osteochondromas, which can be solitary or multiple, sessile or pedunculate.

Psammomatous Meningioma in the Lateral Medullary Cistern

Psammomatous meningiomas (PMs) contain abundant psammoma bodies, which may become confluent and form calcified tumors. It is a rare histologic type of World Health Organization grade 1 meningioma. They are more common in females between the fifth and seventh decades of life. It is usually seen in the spine as an intradural extramedullary lesion surrounding the spinal cord. The frontal region is the most common location for the intracranial PM. It is extremely rare to be found in the lateral medullary cistern. This type of meningioma may arise from arachnoid cap cells in the arachnoidal or pial layers without obvious dural attachment. The MRI findings depend on the degree of calcification. They are isointense or hypointense on T1-w and T2-w images. Unlike ordinary meningiomas, most PMs show moderate and heterogeneous enhancement (►**Fig. 11**).[27] The main differential diagnoses

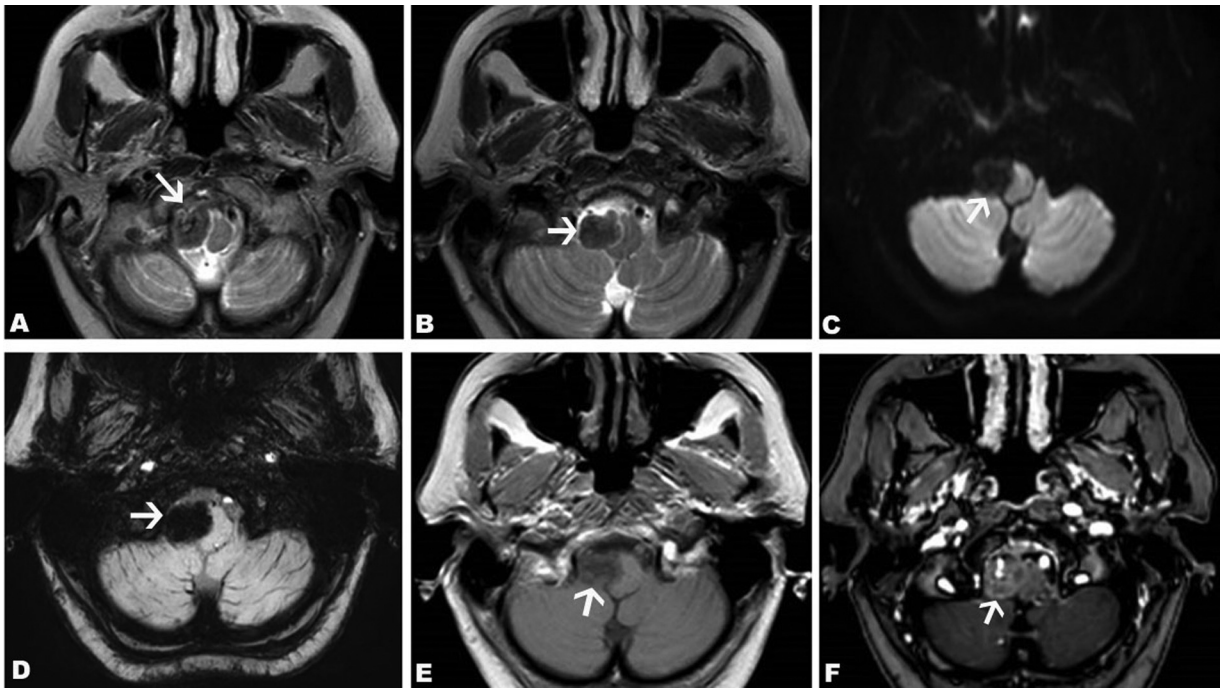

Fig. 11 Magnetic resonance imaging of a skull base psammomatous meningioma in the lateral medullary cistern in a 76-year-old female patient with headache. The mass shows marked hypointensity on axial T2-weighted images (**A**,**B**), diffusion-weighted imaging (**C**), susceptibility-weighted imaging (**D**), and heterogeneous hypointense on T1-weighted image (**E**) (arrows). The lesion reveals moderate enhancement on post-gadolinium-enhanced T1-weighted image (**F**) (arrow). There is encasement of left vertebral artery.

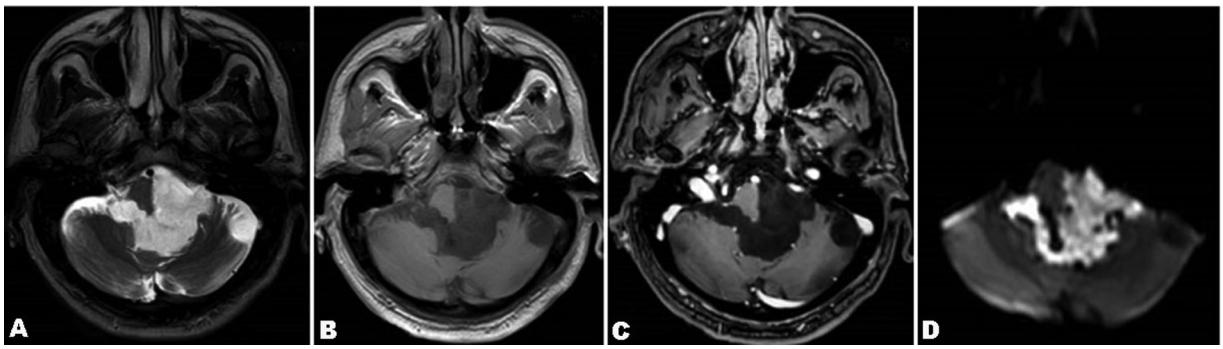

Fig. 12 Magnetic resonance imaging of a pathologically confirmed intraventricular epidermoid tumor in a 34-year-old male patient with headache, ataxia, and blurred vision. (**A**) Transverse T2-weighted image shows an inhomogeneous mass with high signals in the expanded fourth ventricle and bilateral foramen of Luschka (FL). (**B**) The tumor signal intensity is heterogeneous and slightly hyperintense to cerebrospinal fluid on transverse T1-weighted image. The expansion of the fourth ventricle and FL is also well seen. (**C**) Transverse post-gadolinium T1-weighted image reveals no enhancement. (**D**) Diffusion-weighted imaging demonstrates the lesion to be inhomogeneous hyperintense. The lesion is hypointense on the corresponding apparent diffusion coefficient map (not shown), confirming that the diffusion abnormality is due to restricted diffusion.

of the disease include inflammatory pseudotumor (IgG-4 disease), lymphoma, granulomatous infections such as sarcoidosis, and mesenchymal neoplasia. On DWI, lymphoma exhibits restricted diffusion. Increased IgG-4 levels may help to diagnose inflammatory pseudotumor. Neurosarcoidosis usually shows leptomeningeal and/or pachymeningeal diffuse or nodular thickening and enhancement on imaging. Mesenchymal neoplasia may be indistinguishable based on MRI alone.

Epidermoid Cyst

Epidermoid cysts or pearly tumors can arise from the inclusion of the ectodermal epithelial elements during neural tube closure. Epidermoid cysts account for up to 1% of all primary intracranial tumors. Fourth ventricle epidermoid cysts may insinuate through the FLs with expansion and extend into the CPA (►**Fig. 12**).[28] These cysts grow very slowly, so the onset of symptoms and signs can manifest over a period of months to years. Intracranial epidermoid cysts generally appear hypodense on CT. MR imaging demonstrates inhomogeneous hypointense T1 signal and inhomogeneous hyperintense T2-FLAIR signal intensities. They typically do not enhance, but may sometimes show minimal and peripheral enhancement. There is a restricted diffusion on DWI. Hydrocephalus may not be present. Calcification is rarely seen. An epidermoid cyst may be hyperdense (white epidermoid) due to hemorrhage, saponification, or high protein content.[29] The radiological differential diagnoses of an epidermoid cyst include an arachnoid cyst, dermoid cyst, abscess, and a slow-growing brain tumor. Arachnoid cysts follow the CSF signal without restricted diffusion. A dermoid cyst is usually at a more central location with fat and foci of calcification. Abscesses show the typical peripheral contrast enhancement. A slow-growing brain tumor is also without restricted diffusion. The MRI findings of an epidermoid cyst are usually specific for the final diagnosis.[29,30]

Hypoglossal Schwannoma

The hypoglossal nerve originates at the hypoglossal nucleus, passes through the hypoglossal canal, and innervates the

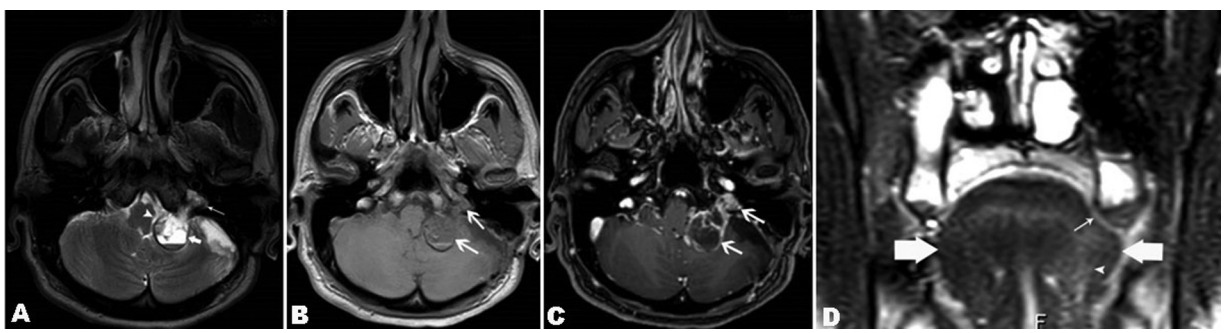

Fig. 13 Magnetic resonance imaging of a pathologically confirmed hypoglossal schwannoma in a 34-year-old man with an uncomfortable sensation on his tongue. (**A**) Transverse T2-weighted image shows a large tumor with a solid component in the enlarged hypoglossal canal and cystic component in the premedullary cistern, extending adjacent to the foramen of Luschka (arrow). The solid parts are heterogeneous hypointense to cerebrospinal fluid (CSF), and the cystic component is isointense to CSF with fluid–fluid level. (**B**) The mass shows heterogeneous hypointense signals on T1-weighted image (arrows). (**C**) Gadolinium-enhanced T1-weighted image reveals nodular and peripheral enhancement in the tumor (arrows). (**D**) Coronal fluid attenuation inversion recovery image reveals the tongue (thick arrows) with left-sided hemiatrophy due to chronic hypoglossal nerve palsy. Notice the fatty infiltration on the left side of the tongue (arrowhead) with prominent contour concavity (arrow).

tongue. Hypoglossal schwannomas can be classified as intradural (intracranial-type A), intra-extracranial (type B), or extracranial (type C). Hemitongue atrophy is the most common and characteristic symptom, but it may also be associated with lower cranial nerve palsy and cerebellar signs. Schwannomas are usually isodense relative to brain parenchyma on a CT scan. Cystic changes or hemorrhage may be seen. Bone-window CT images can demonstrate expansion of the hypoglossal canal. They are isointense or hypointense relative to gray matter on T1-w MR images and slightly hypointense to CSF on T2-w images. They reveal a typically homogeneous enhancement or peripheral enhancement in cystic changes. Hemitongue atrophy with fatty replacement and inhomogeneous enhancement on gadolinium-enhanced MR imaging are the key diagnostic clues for the hypoglossal schwannoma (►**Fig. 13**). The main differential diagnosis of a mass in the hypoglossal canal includes primarily juxtaarticular cysts and hypoglossal canal nonenhancing cystic lesions.[31] In addition, nasopharyngeal carcinoma or a large glomus jugulare mass that has grown into the hypoglossal canal may also be in the differential diagnosis.

Conclusion

Imaging findings of many space-occupying lesions located in or around the FL can be nonspecific. However, some distinctive imaging features combined with clinical data and epidemiologic history can assist the radiologist to narrow the differential diagnosis or, in some cases, make a final diagnosis.

Conflict of Interest Disclosure
The authors declared no conflicts of interest.

References

1 Johal J, Paulk PB, Oakes PC, Oskouian RJ, Loukas M, Tubbs RS. A comprehensive review of the foramina of Luschka: history, anatomy, embryology, and surgery. Childs Nerv Syst 2017;33(09): 1459–1462
2 Tamilchelvan P, Boruah DK, Gogoi BB, Gogoi R. Role of MRI in differentiating various posterior cranial fossa space-occupying lesions using sensitivity and specificity: a prospective study. Cureus 2021;13(07):e16336. Doi: 10.7759/cureus.16336
3 Brandão LA, Poussaint TY. Pediatric brain tumors. Neuroimaging Clin N Am 2013;23(03):499–525
4 Jallo GI, Biser-Rohrbaugh A, Freed D. Brainstem gliomas. Childs Nerv Syst 2004;20(03):143–153
5 Poretti A, Meoded A, Huisman TA. Neuroimaging of pediatric posterior fossa tumors including review of the literature. J Magn Reson Imaging 2012;35(01):32–47
6 Demir MK, Yapıcıer Ö, Mert B, Alshareefi W, Bozbuğa M. Primary Sonic Hedgehog-activated dorsal brainstem medulloblastoma and ipsilateral cerebellar atrophy in an adult. Neuroradiol J 2020;33(01):75–79
7 Zhang S, Ai L, Chen XZ, Wang K. Radiological evaluation of infratentorial gangliogliomas in various anatomic locations of the cerebellum and brainstem. Clin Neuroradiol 2017;27(03):319–327
8 Purohit B, Kamli AA, Kollias SS. Imaging of adult brainstem gliomas. Eur J Radiol 2015;84(04):709–720
9 Brandão LA, Young Poussaint T. Posterior fossa tumors. Neuroimaging Clin N Am 2017;27(01):1–37
10 Yang DX, Jing Y, Xu ZM, et al. Primary glioblastoma of cerebellopontine angle in adult mimicking acoustic neuroma. World Neurosurg 2019;122:48–52
11 Demir MK, Hakan T, Akinci O, Berkman Z. Primary cerebellar glioblastoma multiforme. Diagn Interv Radiol 2005;11(02): 83–86
12 Panigrahi S, Mishra SS, Das S. Primary cerebellopontine angle glioblastoma in an adult. Asian J Neurosurg 2017;12(01):62–64
13 Kasliwal MK, Chandra PS, Sharma BS. Images in neuro oncology: primary extraaxial cerebellopontine angle ependymoma. J Neurooncol 2007;83(01):31–32
14 Ebrahimi H, Jelodar S, Karimi Yarandi K, Eftekhar Javadi A, Alimohamadi M. Adult cerebellopontine angle ependymoma presenting as an isolated cisternal mass: a case report. J Med Imaging Radiat Sci 2020;51(04):689–693
15 Aksoy FG, Gomori JM. Choroid plexus papilloma of foramen of Luschka with multiple recurrences and cystic features. Neuroradiology 1999;41(09):654–656
16 Kim SM, Jung SS, Park MS, Park KS. Meningioma in the lateral cerebellomedullary cistern without dural attachment. J Korean Neurosurg Soc 2010;47(06):464–466
17 Dangouloff-Ros V, Grevent D, Pagès M, et al. Choroid plexus neoplasms: toward a distinction between carcinoma and papilloma using arterial spin-labeling. AJNR Am J Neuroradiol 2015;36 (09):1786–1790
18 Omofoye OA, Binello E. Intraventricular metastases from rectal carcinoma: case report and literature review. J Biomed Res 2019; 34(04):318–322
19 Cummings TJ, Bridge JA, Fukushima T. Extraskeletal myxoid chondrosarcoma of the jugular foramen. Clin Neuropathol 2004;23(05):232–237
20 Tateishi U, Hasegawa T, Nojima T, Takegami T, Arai Y. MRI features of extraskeletal myxoid chondrosarcoma. Skeletal Radiol 2006;35 (01):27–33
21 Yeom KW, Lober RM, Mobley BC, et al. Diffusion-weighted MRI: distinction of skull base chordoma from chondrosarcoma. AJNR Am J Neuroradiol 2013;34(05):1056–1061, S1
22 Woolen S, Gemmete JJ. Paragangliomas of the head and neck. Neuroimaging Clin N Am 2016;26(02):259–278
23 Midyett FA, Mukherji SK. Jugular foramen paraganglioma. In: Skull Base Imaging. Springer, Cham; 2020:189–195. Doi: doi.org/10.1007/978-3-030-46447-9_29
24 Griauzde J, Srinivasan A. Imaging of vascular lesions of the head and neck. Radiol Clin North Am 2015;53(01):197–213
25 Vogl TJ, Bisdas S. Differential diagnosis of jugular foramen lesions. Skull Base 2009;19(01):3–16
26 Osborn AG, Brinton WR, Smith WH. Radiology of the jugular tubercles. AJR Am J Roentgenol 1978;131(06):1037–1040
27 Liu L, Lu Y, Peng W, et al. Imaging features of intracranial psammomatous meningioma. J Neuroradiol 2017;44(06): 395–399
28 Law EK, Lee RK, Ng AW, Siu DY, Ng HK. Atypical intracranial epidermoid cysts: rare anomalies with unique radiological features. Case Rep Radiol 2015;2015:528632. Doi: 10.1155/2015/528632
29 Forghani R, Farb RI, Kiehl TR, Bernstein M. Fourth ventricle epidermoid tumor: radiologic, intraoperative, and pathologic findings. Radiographics 2007;27(05):1489–1494
30 Yuh WT, Barloon TJ, Jacoby CG, Schultz DH. MR of fourth-ventricular epidermoid tumors. AJNR Am J Neuroradiol 1988;9(04): 794–796
31 Weindling SM, Wood CP, Hoxworth JM. Hypoglossal canal lesions: distinctive imaging features and simple diagnostic algorithm. AJR Am J Roentgenol 2017;209(05):1119–1127

